A Physically Based Model for Microstructure Development in a Macroscopic Heat-Affected Zone: Grain Growth and Recrystallization

R.G. THIESSEN and I.M. RICHARDSON

The microstructure in new alloys is increasingly being engineered toward specific properties. Welding, however, alters or destroys this carefully constructed microstructure in the weld and the surrounding region, known as the heat-affected zone (HAZ). Modeling the influence of the entire thermal cycle of the welding process with a physically based model for the material can provide new understanding of the microstructure evolution due to the welding process. In this work, the phase-field method employed uses a physically based model to describe the motion of grain boundaries during welding. Via a unique dual-mesh strategy, calculation times for a macroscopic HAZ are drastically reduced while still maintaining sufficient detail for microstructure characterization.

I. INTRODUCTION

THE thermal cycle associated with welding induces many changes in the microstructure surrounding the fusion zone. Recrystallization and grain growth are both important phenomena that can produce significant changes in the mechanical properties of the material.[1,2] In many classes of materials, including those considered highly weldable, the heat-affected zone (HAZ) develops poor mechanical properties due to processes such as recrystallization and grain growth. Modeling the influence of the thermal cycle on the microstructure evolution in a general, physically based approach can give insight into these processes and their kinetics, as well as lead to guidelines to help control this microstructure evolution. Another advantage of such models is that they are applicable to a wide range of process conditions. Given sufficient thermal information, such a model for the microstructure can provide valid information for various welding processes (arc, laser, hybrid), laser surface treatments, or heat treatments and quenches. Most of the earlier models for recrystallization and grain growth have been based on isothermal results and a phenomenological Arrhenius-type equation (often referred to in the literature as Johnson-Mehl-Avrami-Kolmogorov [JMAK] models), such as that presented by Torres *et al*.[3] However, work by Marthinsen *et al*.[4] showed that the nucleation sites for recrystallization are not truly random nor homogenously distributed, which is a fundamental assumption of JMAK models. In addition, Marthinsen *et al*. showed that for a JMAK model to properly fit experimental recrystallization data, the JMAK exponent would have to be a function of the transformed fraction. Clearly, recrystallization and subsequent grain growth are too complex to describe with two constant parameters. The parameters that result from such studies are of limited value for different isothermal experimental conditions, let alone welding conditions.

One of the few examples in the literature dealing with grain growth in the time scales of welding is the work by Mishra *et al*.,[5] where the Monte Carlo method is used to drive simulations sensitive to various heat inputs. Unfortunately, the material parameters for grain growth are phenomenological and have limited applicability to other alloys.

This work presents a model for the evolution of grain size in the HAZ of welded material. The model is applied to the study of welds in AISI316L. This material is an austenitic stainless steel that is virtually free of solid-state phase transformations, providing a good medium for the exclusive study of recrystallization and grain growth. A finite element model calculates the thermal field and exports this information to phase-field simulations for the microstructure.

II. THEORY OF PHYSICAL PHENOMENA

A. *Moving Interfaces in Metals*

If the movement of an interface is studied at the atomistic level, the mechanism can be visualized as atoms diffusing from one organized lattice structure, through a boundary layer of no distinct structure, and into a new lattice. The process, as presented by Gottstein and Shvindlerman,[6] then consists of the generation of lattice sites in the growing grain (or phase) with an associated disappearance of lattice sites in the shrinking grain (or phase), assuming that vacancies are not created. With these mechanics involved, interface motion is reduced to a diffusion-like process where the interface velocity, v, is a function of the jump distance and jump frequency, expressed as

$$v = d(\Gamma_{\oplus} - \Gamma_{\ominus}), \qquad [1]$$

with d as the atomic distance, $\Gamma_{\oplus}$ being the jump frequency of atoms toward the growing grain, and $\Gamma_{\ominus}$ being the jump frequency of the atoms leaving this grain. These jump frequencies will be different if the Gibbs free energy is not the same on both sides of the interface. It should be noted that although reference will be made to grain boundaries, the following theoretical model is derived in a general manner and is equally applicable to interfaces between phases.

The driving force for the growth of a grain with a lower Gibbs free energy is the difference in the free energy per

R.G. THIESSEN, Graduate Student, is with The Netherlands Institute for Metals Research (N.I.M.R.) Rotterdamseweg 137, 2628 AL, Delft, The Netherlands. Contact e-mail: r.g.thiessen@tnw.tudelft.nl I.M. RICHARDSON, Professor, is with the Delft University of Technology, Department of Materials Science & Engineering, Rotterdamseweg 137, 2628 AL, Delft, The Netherlands.

Manuscript submitted March 10, 2005.

unit volume, or P. The free energy release of one atom moving to the grain of lower free energy is then PV_A, where V_A is the atomic volume (Figure 1). The jump frequency is based on the characteristic vibration of the lattice (Debye frequency, ν_D). For the atoms to actually jump from their current lattice position to a neighboring position, a certain migrational activation energy, Q_m, is required, as represented by the schematic peak and valley distribution of free energy in Figure 1. Frequently, Q_m is assumed to be equivalent to the activation energy for diffusion along grain boundaries, which is approximately half of the activation energy for bulk diffusion, Q_{sd}.[6] Including the influence of this migrational activation energy, Eq. [1] can be rewritten as:

$$v = d\,\nu_D \exp\left(-\frac{Q_m}{kT}\right)\left[1 - \exp\left(-\frac{PV_A}{kT}\right)\right] \qquad [2]$$

For most practical purposes, including recrystallization in heavily cold-worked metals, $PV_A \ll kT$ so that $\left(1 - \exp\left(-\frac{PV_A}{kT}\right)\right) \approx \frac{PV_A}{kT}$ This, together with the assumption that $V_A = d^3$, leads to

$$v = \underbrace{\frac{d^4\nu_D}{kT}\exp\left(-\frac{Q_m}{kT}\right)}_{M} \cdot P, \qquad [3]$$

where the leading terms on the right-hand side make up the so-called mobility, M. The mobility can therefore be expressed as

$$M = M_o \cdot \exp\left(-\frac{Q_m}{kT}\right) \quad \text{where} \quad M_o = \frac{d^4\nu_D}{kT} \qquad [4]$$

The driving force for interface motion, P, has interface and bulk contributions. Contributions from the bulk are based on a free energy difference between the bulk regions separated by the interface, ΔE_{blk}. The interface contribution stems from interface motion that can reduce interfacial area and thus reduce the interfacial energy of the system. The difference in interface energy in the system after interface motion can be expressed as ΔE_{int}. This leads to the general expression for the driving force

$$P = \Delta E_{\text{blk}} + \Delta E_{\text{int}}, \qquad [5]$$

and allows the interface velocity to be described as

$$v = M[\Delta E_{\text{blk}} + \Delta E_{\text{int}}] \qquad [6]$$

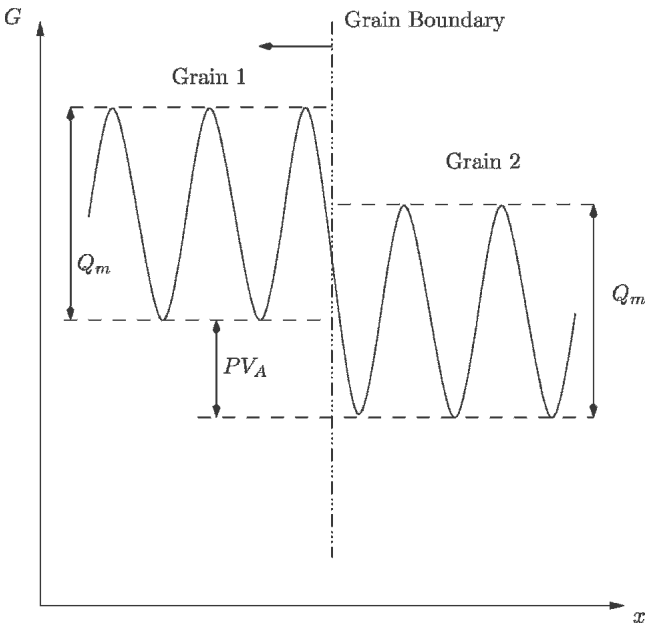

Fig. 1—Schematic representation of the free energy barriers for movement to neighboring lattice sites within one grain, as well as the migration to the more favorable neighbor grain.

B. *Grain Growth*

Given sufficient thermal energy, grain growth will occur, even in the absence of a free energy difference between the bulk of the grains. In such a case, $\Delta E_{\text{blk}} = 0$ and the driving force for interface motion is based solely on the interfacial energy. Thermodynamically, a system with smaller grains has more free energy than a system of the same size with larger grains. This is due to the amount of interfacial area and the associated interfacial energy per unit area, γ. Phase-field methods must quantify this observation locally at each point of interface. This can be elucidated by considering the curved interface of a small sphere in a larger matrix. With no driving force present in the bulk of either side of the interface, the only free energy that can be released by motion of the interface is the interfacial energy. A change in position of the interface results in a change in the volume of the sphere, ΔV, and a change in the area of the interface surrounding the sphere, ΔA. The change in free energy of the system associated with the motion of the interface then becomes

$$\Delta E_{\text{int}} = -\gamma \cdot \frac{\Delta A}{\Delta V} \qquad [7]$$

Expressing $\Delta A/\Delta V$ as the local curvature, κ, yields

$$P = \Delta E_{\text{int}} = -\gamma \cdot \kappa \qquad [8]$$

This implies that the velocity of the interface, from the perspective of the small sphere, is negative and the size of the sphere will decrease. From the perspective of the surrounding matrix, the velocity is positive. Figure 2 depicts how the influence of curvature will drive grain growth in a schematic microstructure. Growing grains with microscopically negative curvatures are often observed experimentally.[6]

The influence of lattice misorientation at the grain boundary on the mobility remains disputed in the literature.[2] For ultra-pure materials, mobility between low-angle grain boundaries appears low and then oscillates with increasing misorientation. For industrial-grade materials, the oscillatory behavior in mobility is not evident. Marx *et al.*[7] developed a cellular automaton method to include the influence of grain boundary angle in the mobility. Grain boundary angles within 5 deg of an optimal angle were given a mobility five times that of other grain boundaries. Most examples in the literature do not assume such a strong dependence of mobility on grain boundary misorientation. Most sources in the literature quote variances of 0 pct to 30 pct in the enthalpy associated with grain boundary migration for

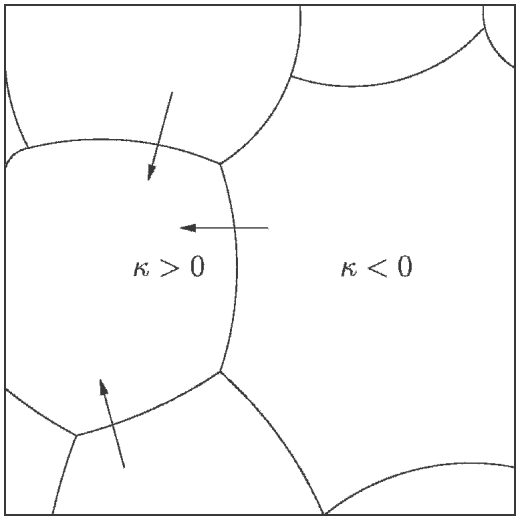

Fig. 2—A typical microstructure in which the large grain on the right has a mesoscopically positive curvature but a microscopically negative curvature.

misorientation angles greater than 20 deg.[2,6] In the model developed here, this small variance is considered to be on the same scale as errors in the estimation of the aforementioned parameters. In this light, an average grain boundary misorientation is assumed for all interfaces.

C. *Recrystallization*

During recrystallization, contributions from the bulk to the driving force for interface motion are no longer negligible. The bulk property in question is the stored strain energy, E_ε. Assuming recrystallization can completely release this stored strain energy, the difference in bulk free energy between a grain that has not recrystallized and a recrystallized grain can be expressed as

$$\Delta E_{\text{blk}} = E_\varepsilon \qquad [9]$$

Contributions to the driving force from the interfacial energy are still active, leading to the expression for the interface velocity:

$$v = M[E_\varepsilon - \gamma \cdot \kappa] \qquad [10]$$

Differences in stored strain energy across a grain boundary can cause a small recrystallized grain to grow, despite its exhibiting an unfavorable interface curvature.

The classical treatment of recrystallization characterizes it as a process of nucleation and growth.[1,8] The general consensus currently, however, is that recrystallization does not occur by means of classical nucleation but rather involves the transformation and growth of "preformed nuclei" or subgrains,[2,9] the size of which can be several micrometers. The location of a transforming subgrain is also determined by the position where the least amount of new interface will be introduced. Therefore, the most thermodynamically favorable location is a subgrain that lies next to an existing grain boundary or triple (and higher-order) junction.

Because of varying orientations with respect to the applied stress, some grains have activated slip systems aligned with the stress and allow the dislocations to pass through the crystal, while other grains must accommodate the stress via significant lattice distortion. This leads to different amounts of strain energy in different grains, with the grains having a higher stored energy being most likely to host initial recrystallization. If atoms have sufficient thermal energy, the lattice can recover, which is generally the case during hot working. This leads to the association of stored strain energy with the amount of cold work performed on the material. Material that undergoes a heat treatment following cold working can also go through a recovery process. The degree to which a material recovers is dependent on the temperature and holding times of the heat treatment, but is also dependent on the stacking fault energy of the material. According to dislocation theory, a low value of the stacking fault energy, γ_{SFE}, hinders dislocation climb and cross-slip[2] and thereby slows the recovery process. AISI316L demonstrates a low value of γ_{SFE}*, also manifested by its creep-resistant behavior.[2,10]

*The stacking fault energy of austenitic steels is ≈20 mJ m^{-2}, compared to ≈170 mJ m^{-2} for aluminum and ≈80 mJ m^{-2} for copper.[8]

Values for the stored strain energy can be obtained through calorimetric experiments comparing the energy necessary to heat a sample that has been cold-worked to the energy necessary to heat an annealed sample.[11] In the absence of calorimetric measurements, theoretical estimates using the dislocation density can be made. The dislocation density ρ, has been shown[2] to be related to the material shear modulus G, Burgers vector b, and yield stress σ_y via

$$\rho = \left(\frac{2\,\sigma_y}{Gb}\right)^2 \qquad [11]$$

The stored strain energy, E_ε, is then derived as

$$E_\varepsilon = \frac{1}{2}\rho\, G\, b^2 \qquad [12]$$

III. PHYSICAL EXPERIMENTS

AISI316L (by wt pct, Cr 16.6, Ni 10.5, Mo 1.8, Mn 1.3, Si 0.3, C < 0.03) was received as 2-mm sheet. In standard production, such sheet material is cold-rolled and subjected to a stress-relief and stabilize (SRS) heat treatment. The SRS heat treatment involves heating samples to 1158 K for 2 hours followed by a slow cool to 948 K before oven-cooling to room temperature, which allows the material to undergo partial recovery.[10] Samples were sheared into 100 × 120-mm sections. To observe grain growth rates without initiating recrystallization, a set of samples received an additional SRS heat treatment and are referred to as partially recovered samples in this work. A second set of samples was annealed. The annealing heat treatment involved heating to 1373 K for 2 hours and a subsequent oven-cool. Since the annealing heat treatment is designed to initiate recrystallization, these samples are referred to as recrystallized. The thermal cycles of the SRS and the anneal treatment are compared with the thermal cycle experienced by a material point 100 μm from the fusion line during gas-tungsten-arc (GTA) welding in Figure 3. A third set of as-received samples served as the control set.

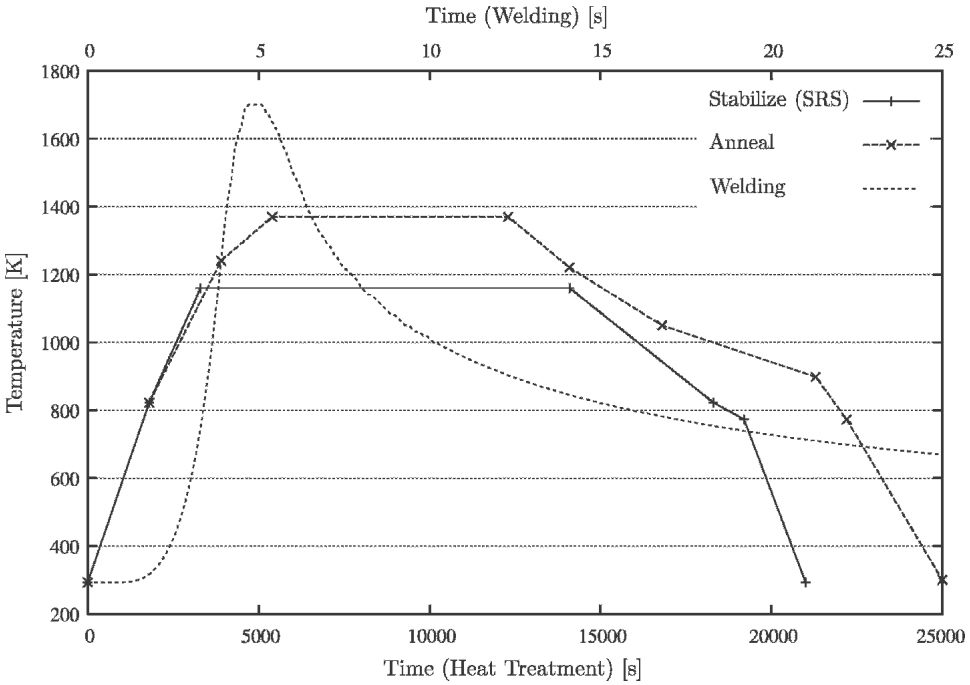

Fig. 3—Comparison of thermal cycles for experimental heat treatments and a calculated thermal cycle for a point 100 μm from the fusion line during welding. The time scale in both heat treatments is three orders of magnitude larger than in a typical welding thermal cycle.

Table I. Welding Process Parameters

Welding electrode: W-2 pct Th	Electrode diameter: 2.4 mm
Torch polarity: DCEN	Electrode tip angle: 60°
Shielding gas: Argon	Flow rate: 10 l min^{-1}

GTA welds were made on three partially recovered samples, three recrystallized samples, and three as-received samples. The welding power was 350 W (35 A, 10 V) and the constant welding velocity was $v_w = 2$ mm s^{-1}. Other welding parameters are listed in Table 1. These parameters led to welds of partial penetration, a typical example of which can be seen in Figure 4. Before welding, the surfaces of partially recovered and recrystallized samples were polished with 240-grit sanding paper to remove the oxide layer. All surfaces were cleaned with alcohol immediately prior to welding.

Cross-sections of the weld and HAZ microstructure were made perpendicular to the welding direction. The final polishing step was made with a 0.06-μm diamond polishing compound and etched with diluted Villela (10 mL HNO_3, 20 mL HCl, 30 mL glycol) for 25 minutes. Grain sizes were measured via the chord intersection method[12] with chords oriented parallel to the fusion line.

IV. MODEL CONSTRUCTION

Physically based modeling of the entire HAZ is a computationally formidable task. A strategy has been proposed to simulate a semicontinuous representation of the microstructure via discrete microstructure domains at the nodal points of a macroscopic finite element mesh.[13,14] By calculating discrete points in the microstructure rather than a single, continuous microstructure, only a fraction of original microstructure needs to be modeled. Earlier studies showed that calculation times are directly proportional to the area of the calculated domain, leading to a significant reduction in calculation times with this dual-mesh strategy. The temperature, thermal gradient, and heating or cooling rates are calculated with the finite element mesh and imposed as boundary conditions on microstructure calculations. The thermal calculations use a double-ellipsoid surface flux based on the Goldak volume source[15] and are performed in a commercially available finite-element code.[16] A total heat flux of 350 W with an efficiency of 90 pct is used to calculate the thermal conditions generated during autogenous arc welding described in Section III. The thermal model has undergone extensive experimental validation for use with AISI316L.[17] The microstructure calculations, the focus of this work, were carried out with phase-field simulations.

The core of the phase field model is based on the definition of a so-called state variable over the entire computational domain. It can be dependent on composition, orientation, or long-range atomic order. The phase-field method has also been adapted for multiple phase calculations, which have been addressed in the literature.[13,18] This concept allows each grain to have uniquely defined properties, such as the value of stored strain energy. The multiphase phase-field code used here, MICRESS, was developed by ACCESS e.V., Aachen, Germany.

Material properties at the microscopic level are derived via the theoretical considerations presented in Section II. The migrational activation energy, Q_m, is based on the activation energy for self-diffusion in austenitic iron, Q_{sd}, which has been measured to be approximately 300 kJ mol^{-1}.[2,19] This activation energy is expected to be slightly higher for AISI316L due to the restricted mobility of the large

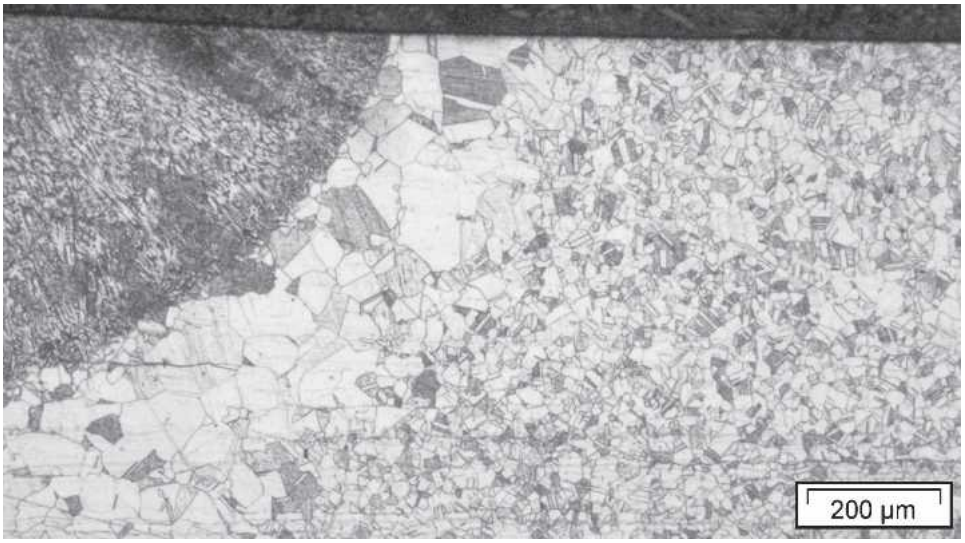

Fig. 4—A typical cross-section of an as-received sample after being welded. The small, equiaxed grains on the right are representative of the material in the as-received condition. During welding, microstructure far from the heat source is not provided with enough thermal energy to evolve and remains unchanged. Closer to the heat source, the microstructure can evolve via mechanisms such as grain growth and recrystallization. The darker zone in the upper-left corner indicates the region that was liquified and is characterized by a completely new, dendritic microstructure.

alloying atoms, such as Mo. This knowledge delivers a reasonable estimate for Q_m of 150 to 200 kJ mol^{-1}, but the final value for use in the material model ultimately should be derived from experimental results. The mobility is implemented using the dependency on temperature as presented in Section II–A with a value for d of 2.6 Å and for ν_D of $6 \cdot 10^{13}$ Hz. Using typical mechanical property values for AISI316L in the as-received state ($G = 75$ GPa, $\sigma_y = 300$ MPa) and Eqs. [11] and [12], a dislocation density of $\rho_{disl} = 10^{15}$ m^{-2} is derived, leading to a stored strain energy of $E_\varepsilon = 2.4\ 10^6$ J m^{-3}. The value for the grain boundary energy is based on the published value for AISI304[8] of $\gamma_{gb} = 0.835$ J m^{-2}. Following the considerations of recrystallized grains nuclei actually being subgrains with highly localized deformation, nuclei are given an initial size of 3 μm. The initial grain size is set to 15 μm to match with experimental measurements in the base material, as shown in Figure 4. To avoid undesired influence from boundary conditions of the simulated microstructure, a minimum domain size is required. This minimum size for recrystallization and grain growth calculations is related to the final grain size. Through convergence studies, it was found that the final microstructure should host at least 60 grains to avoid unnatural influences from boundaries. This implies a minimum domain size of 305×305 μm^2 for the as-received HAZ simulations and 385×385 μm^2 for the simulations of the HAZ in the partially recovered samples. These domains, oriented parallel to the fusion boundary, are then subject to calculated thermal cycles at 100, 150, 200, and 350 μm from the fusion line.

V. RESULTS AND DISCUSSION

The grain growth model, based on the temperature-dependent grain boundary mobility, was based on the theory presented in Section II–B. The SRS heat treatment provided the ideal setting to examine grain growth without the significant release of strain energy associated with recrystallization. A truly temperature-dependent model should be valid for both the long holding times of the heat treatment as well as the short, intense growth periods associated with welding. The one value that was difficult to determine *a priori* was the activation energy for atomic migration, Q_m. The activation energy for self-diffusion, Q_{sd}, of pure austenitic iron is 300 kJ mol^{-1} and would suggest a theoretical value for Q_m of 150 kJ mol^{-1}. The composition of AISI316L involves, aside from Cr and Ni, a significant amount of Mo, which reduces grain boundary mobility. Macroscopically, this is manifested in the measurable anticreep properties of AISI316L.[10] Although a major component of creep is the sliding of grain boundaries along each other, the ability of a microstructure to accommodate this motion is directly related to the mobility of the grain boundaries themselves. Therefore, the value of Q_m was expected to be higher than the estimated value based on the theoretical considerations for pure iron. Comparison with experimental results led to an activation energy of $Q_m = 197.5$ kJ mol^{-1}. The mobility calculated here ranges from $M_{(900\ K)} = 7.8\ 10^{-9}$ cm^4 (Js)$^{-1}$ to $M_{(1600\ K)} = 4.5\ 10^{-4}$ cm^4 (Js)$^{-1}$ and produces finite growth kinetics that are appropriate for heat treatments as well as the growth associated with the short thermal cycles characteristic of welding.

The recrystallization component of the model presented in Section II–C was also implemented according to the given theory; however, the recrystallization temperature and the nucleation density could not be gleaned from theoretical considerations and relied on experimental observation and deductive reasoning. The recrystallization temperature is not characteristic of the material *per se*, but strongly dependent on the mechanical and thermal history that the material has experienced.[1,2,6] From the heat-treatment experiments, abnormal grain growth associated with recrystallization was not observed in the partially recovered samples, which stayed

below 1158 K (SRS heat treatment). From these and the annealing results, it can be concluded that the temperature at which recrystallization is initiated lies between 1158 K and 1373 K. From the location of the material point furthest from the fusion zone to display evidence of recrystallization and interpolation within the calculated thermal field, the recrystallization temperature was estimated to be 1300 K.

Considering the nucleation density of recrystallized grains led to a serendipity of the usually challenging, highly inequilibriated thermal cycles associated with welding. Assuming that recrystallization indeed takes place next to the weld pool, the final grain density next to the weld pool is in fact the ideal location to measure nucleation density, since secondary grain growth has minimal time to develop. This allowed the final grain density at approximately 100 μm from the fusion line in an as-received sample to be directly used as the nucleation density for recrystallization. At distances of less than 100 μm from the fusion line, larger grains are often partially melted. From analysis of micrographs, the nucleation density in the analyzed surface was estimated as $\rho_{\text{nuc}} = 5.77\ 10^{-4}\ \mu\text{m}^{-2}$.

This nucleation density was used for the calculations of the annealing heat treatment. The microstructure was modeled with an initial grain size of 15 μm. Nucleation of recrystallized grains occurred once the sample had reached 1300 K, which occurred after 4500 seconds. As seen in Figure 5(a), the newly nucleated grains contributed to a temporary drop in the average grain size, a more detailed view of which is shown in Figure 5(b). This was followed by a period of strong growth that continued until the recrystallized grains impinged against one another. After impingement, the microstructure followed standard grain growth until the heat treatment came to an end and the sample was cooled. Once the sample cooled to below approximately 1000 K, further grain growth ceased.

The final calculated microstructure, as well as the experimental, exhibited a significant range in grain sizes. The measured grain sizes from the experimental heat treatments are shown, with error bars, on the right of Figures 5(a) and 6(a). This range in grain sizes has consequences for the measured grain size in the HAZ of samples that were subsequently welded. Experimental measurements in Figure 6(b) show higher growth close to the fusion line than the calculated microstructure. Although the actual microstructure in the partially recovered samples started with a large range of grain sizes, the simulations start with a relatively homogenous grain size distribution. It is likely that the apparent additional growth close to the fusion zone in the experimental welds is due to very small grains being consumed. This growth could be enforced during simulations by starting with a microstructure with a broader range of grain size.

As-received samples, on the other hand, started with an equiaxed microstructure with very little variation in the measured grain sizes. This allowed the simulations with a homogeneous grain size distribution to be more representative of the initial experimental conditions. Figure 7(a) shows the growth kinetics of various positions in the HAZ of the simulated as-received sample. The apparent reduction in the average grain radius at 0.5 seconds is due to the nucleation of recrystallized grains. Once the recrystallized grains reach the boundaries of the parent grain, an increase in the average grain radius is noticed. The growth curve for grains at 100 μm from the fusion line in Figure 7(a) shows the impingement of recrystallized grains after approximately 1 second of growth. Further from the fusion line, the lower growth rate is due to the temperature-dependent mobility reduction as the work piece cools. Figure 7(b) depicts the measured grain diameters from the experimental welds as well as the calculated grain sizes.

The modeled microstructure morphology for a material point 150 μm from the fusion zone is shown in Figure 8. Figure 8(a) shows the initial microstructure, with lighter shading representing higher amounts of stored strain energy, E_ε. Figure 8(b) shows the microstructure at $t = 0.5$ seconds,

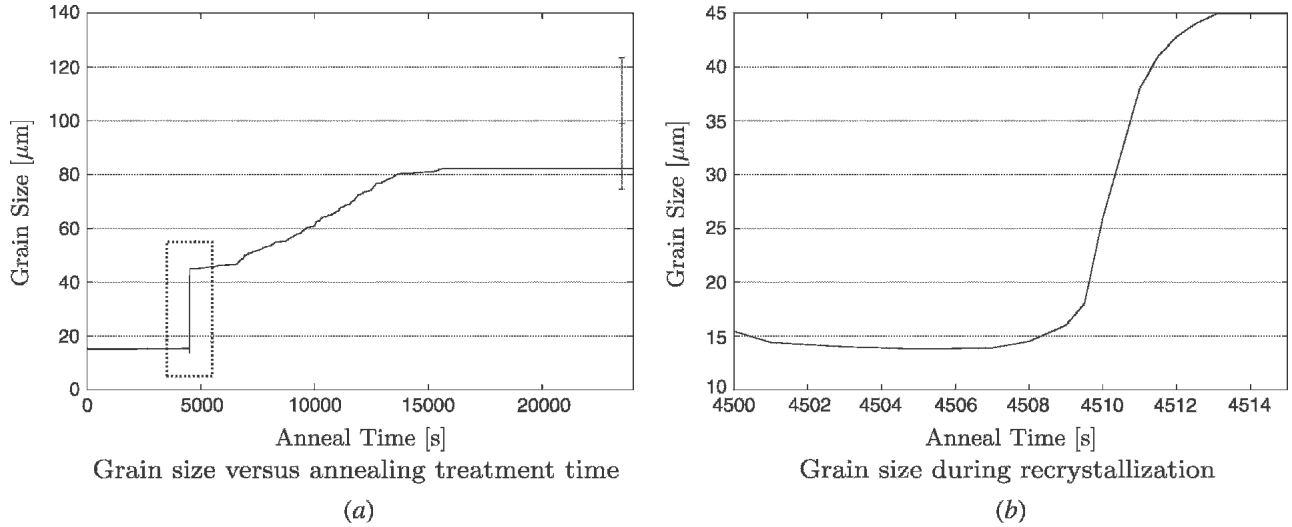

Fig. 5—(*a*) Calculated average grain size evolution during the annealing heat treatment. The high growth rate (in the dashed box, magnified in (*b*)) during recrystallization is followed by a period of secondary grain growth. The upper plateau corresponds to the time range at which the sample cools and the temperature-dependent mobility is reduced. The final measured grain size is shown with error bars. (*b*) A more detailed view of the calculated growth kinetics during recrystallization. A reduction in the average grain size is observed with the introduction of new, recrystallized grains. The high growth rate is reduced once recrystallized grains impinge against one another.

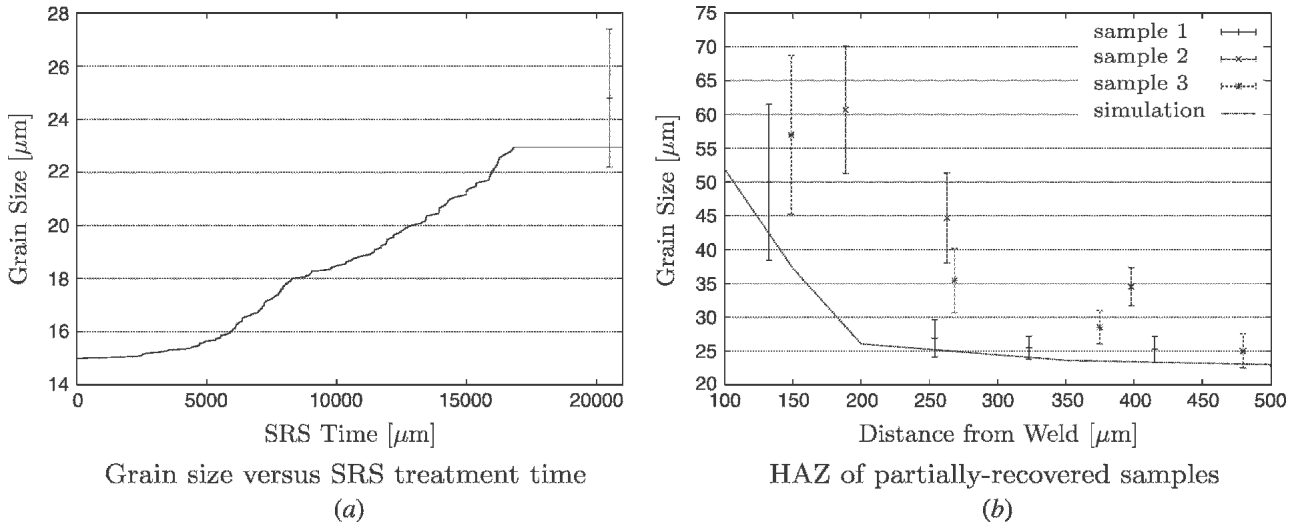

Fig. 6—(*a*) Average grain size as a function of the SRS heat treatment time. The data point with error bars represents experimental measurements of the final microstructure. (*b*) Grain size *vs* distance from fusion line in the GTA welds of the partially recovered samples. Simulation results are joined by the solid line.

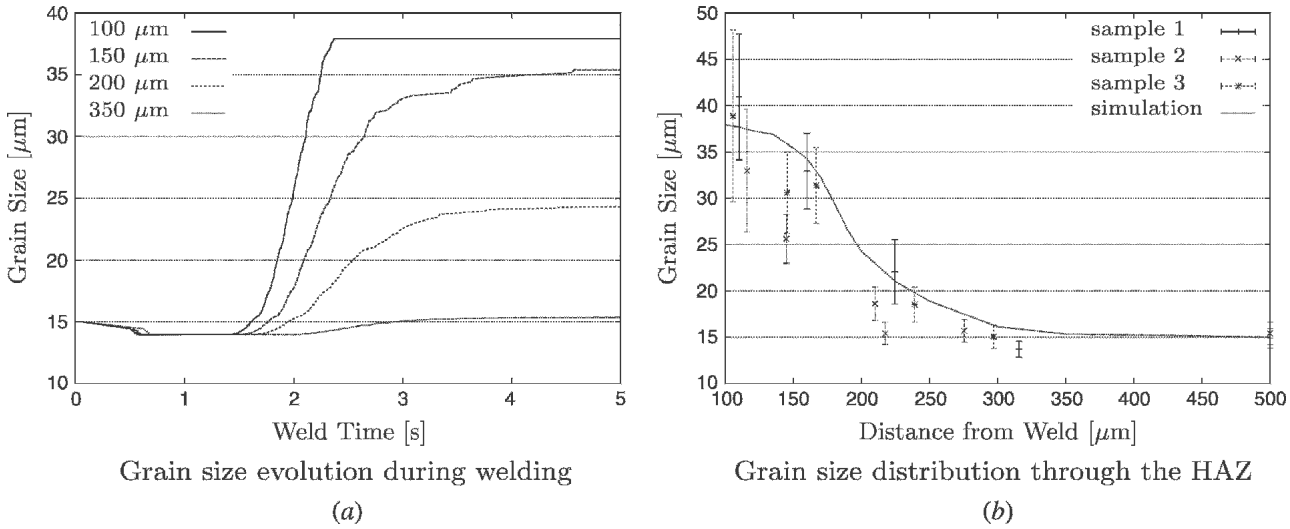

Fig. 7—(*a*) Calculated average grain size at given distances from the fusion line *vs* welding time. A reduction in the average grain size is observed with the nucleation of new grains. (*b*) Grain size *vs* distance from fusion line in the GTA welds of the as-received samples. Simulated grain size values are joined with a spline approximation line.

as the first recrystallized grains appear along grain boundaries and triple junctions of grains with the highest stored strain energy. Here and in the following figures, the nonhomogeneous distribution of recrystallized grains is in agreement with the observations of Marthinsen *et al.*[4] and distinguishes this model from standard JMAK models. Figure 8(c), at $t = 1.4$ seconds, shows the recrystallized grains reaching the approximate size of the original microstructure. Another important feature of these simulations, and a distinction from JMAK models,[2] is the ability to represent nonisotropic growth of recrystallized grains, driven by the distribution of stored strain energy. This is determined by the initial stored strain energy distribution, which in turn dictates the degree with which free energy can be released *via* recrystallization in a given direction. The nonisotropic growth can be seen in Figure 8(d) ($t = 2.0$ seconds) and the following frames. At $t = 2.5$ seconds, impingement of the recrystallized grains against one another begins to have a damping effect on the growth kinetics (Figure 7(a)), and the microstructure evolves into one with longer, flatter interfaces (Figure 8(e)). Figure 8(f) shows the final microstructure.

VI. CONCLUSIONS

An integrated macro/micro, physically based model for the microstructure development in a macroscopic HAZ has been presented. By comparing the growth kinetics near the weld pool with growth during prolonged heat treatments, it may be concluded that a second growth mechanism, recrystallization, is activated and plays an important role in grain growth near the fusion zone of the welded as-received

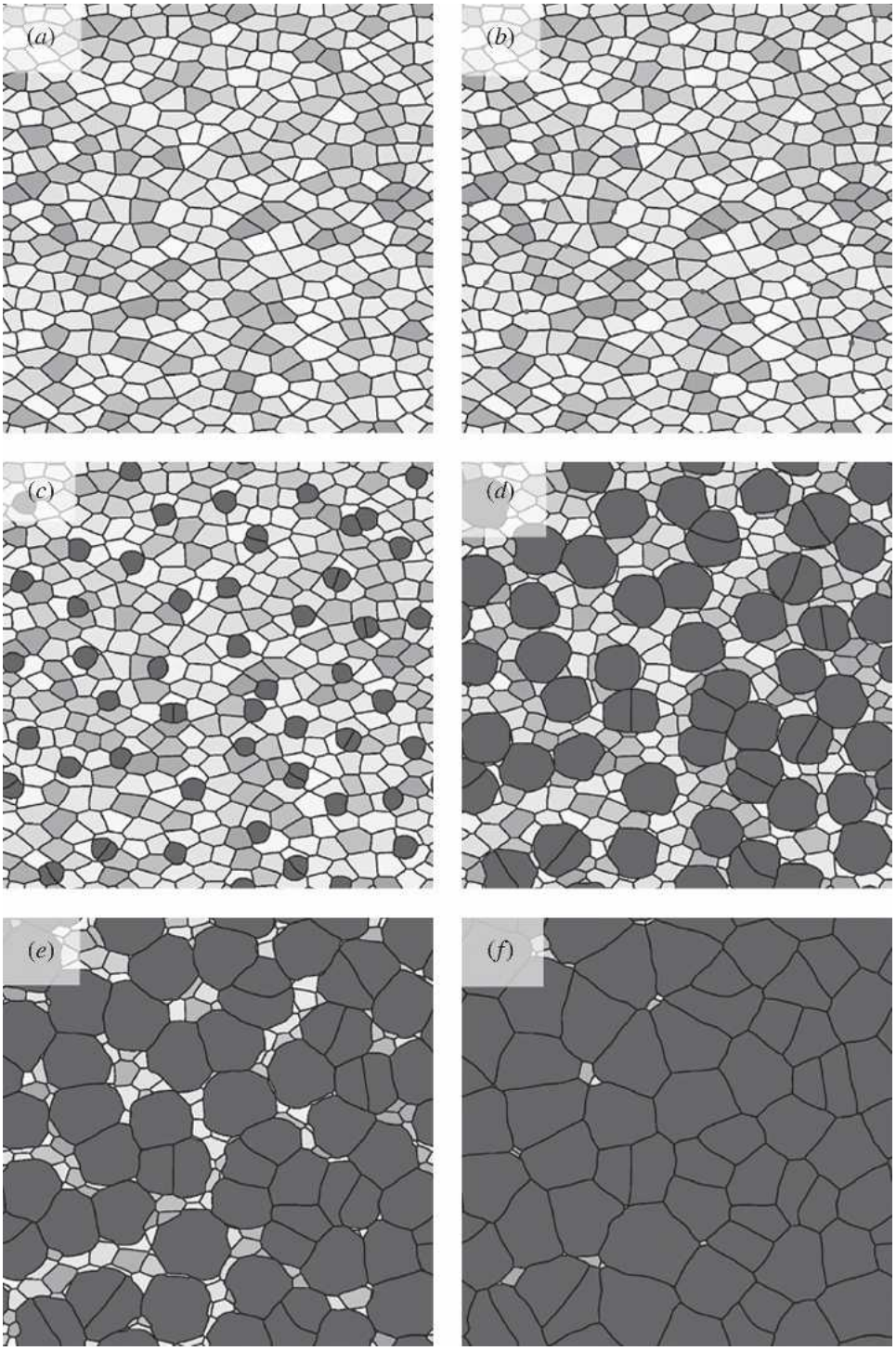

Fig. 8—Representations of the microstructure at 150 μm from the fusion line for various times through the welding thermal cycle (from left to right, top to bottom). Shading in the figures indicates amount of stored strain energy, with darker shading representing lower values of stored strain energy. (*a*) Initial microstructure. (*b*) The first signs of recrystallization at $t = 0.5$ seconds. (*c*) At $t = 1.4$ seconds, recrystallized grains have reached the approximate size of the original grains. (*d*) At $t = 2.0$ seconds, distinctly nonuniform growth has occurred in the calculated plane as a result of the distribution of stored strain energy. (*e*) At $t = 2.5$ seconds, impingement of recrystallized grains has significantly slowed further grain growth. (*f*) Final microstructure.

material. Values for the interface mobility have been derived in a general manner, making the model construction applicable to other alloys. The stored strain energy has been deduced from theoretical considerations, while nucleation density of recrystallized grains was deduced from experimental heat treatments and welds. The strategy proposed here offers significant calculation time savings while still delivering detailed morphology of the microstructure.

Due to the physical basis and generality of the model, the considerations presented here are applicable to the modeling

of different alloys as well as different thermal processes. With appropriate thermodynamic information, the model can also be used for modeling the fraction and morphology of phase transformations during arbitrary thermal processes. Coupling phase transformations with recrystallization and grain growth will provide a more complete understanding of the evolution of microstructure and mechanical properties in material subject to thermal processes.

ACKNOWLEDGMENTS

This research was carried out under project number MC8.01092 (Numerical Modelling of Welded Material) in the framework of the Strategic Research Programme of the Netherlands Institute for Metals Research in The Netherlands. The authors gratefully acknowledge Dr. J. Sietsma of the MCM Group at the TU Delft, whose experience in materials science provided a springboard for many fruitful discussions.

REFERENCES

1. R.E. Reed-Hill and R. Abbaschian: *Physical Metallurgy Principles,* 3rd ed. PWS Publishing Company, Boston, 1994.
2. F.J. Humphreys and M. Hatherly: *Recrystallization and Related Annealing Phenomena,* Pergamon, Oxford, 1996.
3. C.E.R. Torres, F.H. Sanchez, A. Gonzalez, F. Actis, and R. Herrera: *Metall. Mater. Trans. A*, 2002, vol. 33 (1), pp. 25-31.
4. K. Marthinsen and N. Ryum: *Acta Mater.*, 1997, vol. 45 (3), pp. 1127-36.
5. S. Mishra and T. DebRoy: *Acta Mater.*, 2004, vol. 52 (5), pp. 1183-92.
6. G. Gottstein and L. Shvindlerman: *Grain Boundary Migration in Metals,* CRC Press, Boca Raton, FL, 1999.
7. V. Marx, F.R. Reher, and G. Gottstein: *Acta Mater.*, 1999, vol. 47 (4), pp. 1219-30.
8. L. Murr: *Interfacial Phenomena in Metals and Alloys,* Addison-Wesley, Reading, MA, 1975.
9. E.A. Holm, M.A. Miodownik, and A.D. Rollett: *Acta Mater.*, 2003, vol. 51 (9), pp. 2701-16.
10. J. Douthett: in *ASM Handbook,* Davis, J., ed., vol. 4. ASM International, 1998.
11. G. Gottstein, H. Steffen, W. Hemminger, G. Hoschek, K. Broxtermann, H.G. Grewe, and E. Lang: *Scripta Metall.*, 1975, vol. 9 (7), pp. 791-96.
12. E.E. Underwood: in *ASM Handbook,* vol. 9. ASM Materials Park, 1985, pp. 123-24.
13. R. Thiessen and I.M. Richardson: in *Numerical Analysis of Weldability, 7,* H. Cerjak, H.K.D.H. Bhadeshia, eds., Graz, Austria, TU Graz Publishing, 2005, pp. 151–78.
14. R.G. Thiessen and I.M. Richardson: *Metall. Mater. Trans. B,* 2006, vol. 37B, pp. 293–300.
15. J. Goldak, A. Chakravarti, and M. Bibby: *Metall. Trans. B*, 1984, vol. 15 (2), pp. 299-305.
16. *Manual Technical Report*, MSC Software Corporation, 2003.
17. E.M. van der A: M.Sc. Thesis, TU Delft, 2002.
18. I. Steinbach, F. Pezzolla, B. Nestler, M. Seeßelberg, R. Prieler, G.J. Schmitz, and J.L.L. Rezende: *Physica D*, 1996, vol. 94 (3), pp. 135-47.
19. A. Heiming, K.H. Steinmetz, G. Vogl, and Y. Yoshida: *J. Phys. F*, 1988, vol. 18 (7), pp. 1491-503.